Shipboard Radar Rainfall Patterns within the TOGA COARE IFA

David A. Short,* Paul A. Kucera,+ Brad S. Ferrier,#
John C. Gerlach,@ Steven A. Rutledge,& and Otto W. Thiele*

ABSTRACT

Radar rainfall measurements over the equatorial western Pacific warm pool were collected by two shipboard Doppler radars as part of the Tropical Oceans Global Atmosphere Coupled Ocean–Atmosphere Response Experiment during the intensive observing period (November 1992–February 1993). A comprehensive dataset of gridded rainfall fields, convective/stratiform identification maps, and vertical structure products has been produced, covering an area approximately 400 km (E–W) by 300 km (N–S) within the Intensive Flux Array (IFA), centered near 2°S, 156°E. The radar rainfall product, which was used as validation for the Third Algorithm Intercomparison Project of the Global Precipitation Climatology Project, indicates an overall average of 4.8 mm day^{-1}; however, correction for range dependence increases the total to 5.4 mm day^{-1}. Rainfall patterns varied considerably during the experiment with isolated convection dominating periods of light winds, while squall lines and organized mesoscale systems were abundant during two westerly wind bursts. An area-average rainfall of 9.9 mm day^{-1} was observed during the active 2-week period at the end of December, while 0.4 mm day^{-1} was observed during the quiescent week of 2–8 February. The eastern portion of the IFA received the most rainfall with localized maxima exceeding 16 mm day^{-1} for the most active 3-week period. Comparison of daily radar rainfall totals with those observed by an optical rain gauge (ORG) on the 2°S, 156°E buoy shows ORG totals to be systematically higher, by a factor of 2.5. The discrepancy results from a higher average rainfall rate, when raining, as reported by the buoy ORG. However, rainfall rate statistics from the ORGs on the research vessel *Xiang Yang Hong #5* and from its radar are in excellent agreement under the following conditions: 1) the ship is drifting, and 2) the radar data are in the near vicinity of the ship (3–7 km).

1. Introduction

Determination of the freshwater flux from the atmosphere to the ocean was among the specific objectives of the ocean–atmosphere interface component of the Tropical Oceans Global Atmosphere Coupled Ocean–Atmosphere Response Experiment (TOGA COARE; Webster and Lukas 1992). As a result, the planning for TOGA COARE included a comprehensive strategy in which precipitation estimates could be made from a variety of observations and algorithms. The report of the Fourth Workshop of the TOGA COARE Air–Sea Interaction (Flux) Working Group (Bradley and Weller 1996) details recent progress in the refinement and intercomparison of precipitation estimates within the Intensive Flux Array (IFA) from numerous investigators.

Their data sources include wind, temperature, and humidity observations from the atmospheric sounding network (Parsons et al. 1994) that have been used to determine heat and moisture budget methods with precipitation estimated as a residual term (Lin and Johnson 1996; Frank and Wang 1996; Lin 1997). Measurements of wind, temperature, and humidity at the atmosphere–ocean interface have been used for calculating ocean–atmosphere fluxes (Weller and Anderson 1996; Anderson et al. 1997), which, when combined with ocean salinity data, allow estimates of rainfall. In situ measurements from rain gauges on

*Laboratory for Atmospheres, NASA, Greenbelt, Maryland.
+Applied Research Corporation, Landover, Maryland.
#Science Systems and Applications, Inc., Lanham, Maryland.
@SPANDAR Radar Facility, NASA, Wallops, Virginia.
&Colorado State University, Fort Collins, Colorado.
Corresponding author address: David A. Short, Code 910, Goddard Space Flight Center, Laboratory for Atmospheres, Greenbelt, MD 20771.
E-mail: short@trmm.gsfc.nasa.gov
In final form 1 August 1997.

ships and buoys have provided point measurements of rainfall rate (R) and total rainfall (Short et al. 1994; Bradley and Paulson 1997). Effects of transient rainfall events on the upper ocean (Gosnell et al. 1995; Esbensen and McPhaden 1996) and relations between the diurnal cycle of rainfall and sea surface temperature (Sui et al. 1997; Webster et al. 1996) have also been reported.

The airborne Doppler radar program provided selected sampling of a wide variety of precipitating clouds and mesoscale systems from both horizontally and vertically scanning radars (Yuter et al. 1995). Lightning observations gave indications of the combined effects of kinematic and microphysical processes in active convection (Peterson et al. 1996). High temporal and spatial resolution measurements of radar reflectivity, Doppler velocity, and spectral width from vertical profilers have also provided detailed observations of the vertical structure and classification of precipitating clouds (Ecklund et al. 1995; Williams et al. 1995; Gage et al. 1996). Raindrop size distribution observations from aircraft (Willis et al. 1995; Yuter and Houze 1997) and an island-based disdrometer (Tokay and Short 1996) have been analyzed to determine algorithms for retrieving rainfall rate (R) from radar reflectivity (Z).

Because of the broad range of time and space scales over which ocean–atmosphere interactions take place (WCRP 1990), continuous monitoring of mesoscale rainfall patterns within the IFA was an integral component of the precipitation measurement program. Description and understanding of the initiation, organization, evolution, propagation, and vertical structure of atmospheric convection was also required to further the understanding of vertical transports of moist static energy and momentum that subsequently modify the environment in which the convection occurs (T. Rickenbach and S. Rutledge 1997, manuscript submitted to *J. Atmos. Sci.*). To address these goals, and to obtain spatially contiguous data, providing context for point measurements from numerous mobile platforms, the comprehensive precipitation measurement program included shipboard C-band Doppler radars, deployed within the IFA during the intensive observation period (IOP), November 1992–February 1993 (TOGA COARE International Project Office 1992).

Two research vessels (R/Vs), the *Xiang Yang Hong #5* (People's Republic of China, hereafter *PRC #5*) and the *John V. Vickers* (United States, hereafter *Vickers*), carried the TOGA and MIT (Massachusetts Institute of Technology) Doppler radars, respectively, in a series of three cruises, providing coverage of the IFA for most of the IOP. Detailed studies of the MIT radar data have been undertaken by several investigators to determine the vertical structure and modulation of convection (DeMott 1996), to provide high spatial resolution estimates of rainfall near the *Vickers* (Doggett 1996), and to relate rainfall production to the horizontal scale and morphology of precipitating systems (T. Rickenbach and S. Rutledge 1997, manuscript submitted to *J. Atmos. Sci.*).

A combined analysis of the TOGA and MIT radar reflectivity data is reported here. Gridded rainfall products, with a spatial resolution of 2 km $\times$ 2 km and a temporal resolution of 10 min, have been derived from approximately 25 000 radar volume scans. The first version of these products, released in November 1994, has been described elsewhere (Ferrier et al. 1995a; Kucera et al. 1995; Short et al. 1995). The present paper describes version 2 algorithms and products, released in November 1995, which were used as validation for rainfall estimates from infrared, visible, and microwave satellite observations retrieved by numerous investigators participating in the Third Algorithm Intercomparison Project (Ebert 1996; Ebert et al. 1997; see also Aonashi et al. 1996) of the Global Precipitation Climatology Project. The version 2 release, which has been statistically analyzed by Polyak et al. (1997), includes adjustments that were made to improve internal consistency of the radar products, increasing overall rainfall rates by 30%–40% over the version 1 release.

Products presently available include maps of rainfall rate and convective/stratiform classification on a fixed latitude–longitude grid within approximately 145 km of either radar, rasterized images for animation, catalog files with summary information for each scan, the raw radar data, software for processing the raw data, and corrected data (see Table 1). Localized subsets of the radar rainfall grid over ship and buoy locations have also been generated in order to facilitate comparison of radar rainfall with in situ data. This includes rainfall rate measurements from optical rain gauges that were mounted on numerous ships and buoys (E. Bradley and C. Paulson 1997, manuscript submitted to *J. Atmos. Oceanic Technol.*). The intercomparison of gauge and radar rainfall is on going. This paper presents a summary of the radar processing procedures, some analyses of the products, limited comparisons with shipboard and buoy-mounted optical rain gauges, and an evaluation of the accuracy of the radar rainfall data.

As a preliminary comment on the accuracy of radar rainfall rates, it must be stated that it is dependent upon a number of factors, most critically the radar calibration, but also including attenuation due to intervening rain along the radar path and water on the radome, the vertical structure of the precipitating systems, spatial variability of rainfall rate within the radar scattering volume, and the reflectivity (Z)–rainfall rate (R) relation [see Austin (1987) and Sauvageot (1994) for complete discussions]. Major tasks in the generation of the radar rainfall products have included a careful examination of calibration results conducted before, during, and after the field experiment, a comparative analysis of measurements from the two radars in the area of overlapping coverage, an analysis of the vertical structure of reflectivity, and a comparison of rainfall rates from radar and rain gauges. Section 2 describes the location and calibration of the radars, section 3 gives details of the data-processing algorithms, section 4 describes rainfall patterns, section 5 presents a discussion of radar–rain gauge comparisons, section 6 presents radar–radar comparisons and error estimates, while section 7 contains a summary of the major results.

2. Deployment, navigation, and calibration

To maximize radar coverage of the IFA throughout the 4-month IOP, the radar ship schedules were staggered with alternating port calls, each ship making three cruises. During each cruise there are about 5 days of single radar coverage at the beginning and end, and a central 20-day period of dual coverage. The three cruises took place during the following time intervals. Cruise 1: 10 November–10 December 1992, cruise 2: 15 December 1992–18 January 1993, and cruise 3: 22 January–23 February 1993. Figure 1 shows the deployment schedules of the *PRC #5* and the *Vickers*. The R/V *Keifu-Maru*, from Japan, was stationed at 0.5°S, 154.5°E 3–17 November, with a 5-cm weather radar on board. An analysis of the *Keifu-Maru* radar data observed during the period 3–16 November 1992 was made by Mori (1995). A comparative analysis of the data from all three radars during early November has been initiated, with preliminary results reported by Oki et al. (1997).

Figure 2 shows the nominal positions of the radar ships within the IFA (note that for cruise 3 the positions of the R/V *Shiyan #3* and the R/V *Kexue #1* were reversed). During periods of single ship deployment, coverage was centered near 2°S, 156°E, near the middle of the instrumented array. Each ship maintained its position in a sequence of drift and repositioning legs, remaining within 25 km of their designated stations. The radar processing and recording system provided antenna attitude and position readouts from the Inertial Navigation Unit (INU), and geodetic position periodically updated from a global positioning system (GPS). Because of errors in the instantaneous GPS positions of about 100 m (Conley 1993), the INU was "loosely coupled" to GPS input. For the TOGA radar system this meant manual updates of the INU using GPS positions at intervals of about 2 h during drift legs and at the beginning and end of each repositioning leg. During special dual-Doppler

TABLE 1. TOGA COARE radar-rainfall products.

Product	Size (MB)	Compressed (MB)	Availability
Rainmaps	1277	60	Online**
Convective/ stratiform maps	1277	60	Online**
GIF images	54	54	Online**
Catalog files	17		Online*
Raw data (SIGMET format)	40 000	40 000	On request*
Corrected data (Universal Format)	160 000	33 000	On request*

*Contact the Goddard Distributed Active Archive Center.
** Available at http://trmm.gsfc.nasa.gov/trmm_office/index.html.

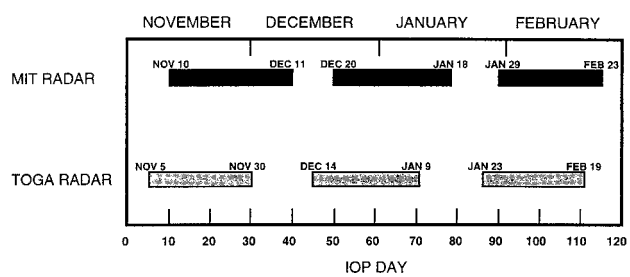

FIG. 1. Deployment schedules (November 1992–February 1993) for the MIT and TOGA radars, aboard the research vessels *JV Vickers* and *Xiang Yang Hong #5*, respectively.

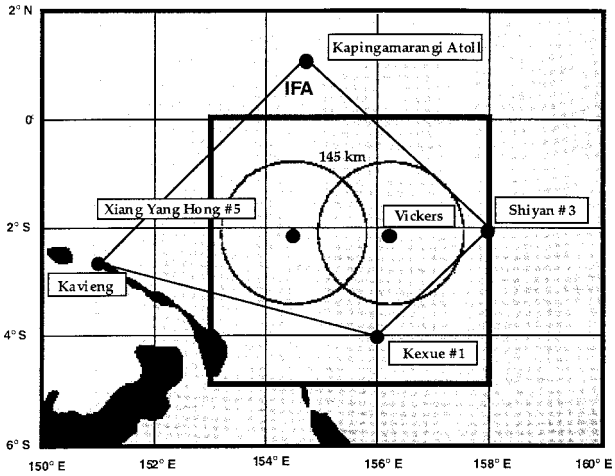

FIG. 2. Nominal deployment positions for the MIT and TOGA radars within the IFA. During single radar coverage periods the nominal position was within 25 km of 2°S, 156°E. Also shown are 145-km range rings, delineating the area covered by the gridded rainfall-rate product. Surveillance scan were taken every 10 min out to a range of 295 km.

operations, TOGA position updates were made every 15 min. TOGA radar positions for each volume scan were then made by linear interpolation of the GPS updates in order to avoid contamination by Schuler oscillations in the INU data (see Masters and Leise 1993). The MIT radar system made automatic GPS updates to the INU positions about every 10 min; however, the loose coupling did allow some adjustment time for the INU. Ship location accuracy is estimated to be ±200 m, although residual contamination by interpolation errors in the TOGA radar positions and Schuler oscillations in the MIT radar INU positions may cause occasional errors as large as 2 km.

Table 2 lists the characteristics of the TOGA and MIT radars. Electronic calibrations of both radars were performed periodically during the field experiment to maintain stability of the systems. Postexperiment determinations of the antenna gain and transmitted bandwidth indicated a gain adjustment of +2.4 dBZ for the MIT radar (T. Rickenbach and S. Rutledge 1997, manuscript submitted to *J. Atmos. Sci.*). However, preliminary examination of the TOGA radar data indicated more complex problems that were largely explained by postexperiment calibration experiments (Ferrier et al. 1995a). For that reason, the MIT radar observations were used as a stable reference for determining final empirical adjustments to the TOGA data.

Several types of corrections were applied to the TOGA radar data, all multiplicative in nature. The four basic types of corrections were related to 1) a malfunctioning amplifier, 2) errors in noise sampling as determined by a radar processor algorithm, 3) hardware and software adjustments, and 4) final empirical adjustments to the MIT radar. Table 3 summarizes each of the four types (C_1 through C_4). Table 4 provides summary statistics of the corrections, including the amount of data affected, the period over which the correction was applied, the average value of the correction, and the minimum to maximum values of the corrections. The following paragraphs give more detailed discussions on the nature of the corrections.

For the TOGA radar a simple power-dependent correction (C_1) was found to be sufficient to correct

TABLE 2. TOGA and MIT radar characteristics.

Parameter	Platform	
	TOGA	MIT
Wavelength (cm)	5.35	5.37
Dynamic range (dB)	80	Same
Minimum detectable signal (dBm)	−105	−109
Peak power output (KW)	250	Same
Pulse width (microseconds)	0.48 (145-km range) 1.82 (295-km range) 1.0 (cruise 3 only)	1.0 (both ranges)
Antenna type	Solid metal parabolic	Same
Reflector size (m)	2.4	Same
Feed type	Horizontally polarized	Same
Antenna gain (dB)	40	Same
Beamwidth (degrees)	1.55	Same
Side lobe level (dB)	−22 to 10° off axis −30 to > 10° off axis	Same

TABLE 3. Summary of corrections applied to TOGA radar data.

Correction	Description
C_1	Malfunctioning log IF amplifier; correction is proportional to returned power
C_2	Errors in noise sampling associated with RVP-6 processing algorithm
C_3	Hardware and software adjustments: • Two-way radome loss (+1.8 dB*Z* throughout IOP) • Changes in measured waveguide loss, antenna gain, and transmitted pulse characteristics (throughout most of IOP). • Variable calibration procedures (cruises 1 and 2) • Unstable behavior in processor (before 18 Nov)
C_4	Final adjustment in TOGA radar calibration obtained by comparing average rainfall from the MIT radar in the overlap area

for a malfunctioning log IF amplifier, described by Ferrier et al. (1995a). Because of hardware changes and power supply fluctuations to the TOGA radar (C_3), the MIT radar was used as the standard for radar–radar comparisons and simple gain adjustments (C_4) were made to the TOGA radar to bring the two into agreement, on the basis of reflectivity measurements and rainfall retrievals in their area of overlap. These gain adjustments were typically held constant for a week or more at a time, until a new adjustment was indicated by a change in the TOGA configuration.

Radar performance parameters were also recorded with each scan. These parameters were used to detect the presence of anomalous scans due to "poor noise samples" and to provide gain adjustments (C_2) for those scans. Noise sampling was performed periodically either before every scan, as in cruises 1 and 2, or every 10–30 min during cruise 3. Noise sampling allows the radar processor to make adjustments for gradual changes in the receiver noise power and offsets in the receiver system. Errors in noise sampling were essentially a result of much larger shifts in the offset of the TOGA radar system interpreted by the radar processor than were actually present. By assuming that the drifts in the noise of the receiver system were small with time, corrections (C_2) were made by subtracting these artificial offsets from the radar data following the algorithm used in the radar processor. Gain adjustments are listed in the catalog files. Details of the objective schemes used for corrections to the TOGA data were reported by Ferrier et al (1995a). A comparison of the echo patterns of 96 distinct cells, observed at the same range from both radars throughout the field experiment (Kucera 1993) provided a statistical database for validation of the adjustments.

Figure 3 (from Ferrier et al. 1995a) shows histograms of reflectivity from the corrected MIT and TOGA radar data for the 96 distinct cells mentioned above. Excellent agreement between the TOGA and MIT radars is seen for reflectivities greater than 20 dB*Z*, corresponding to a convective rainfall rate of 0.88 mm h^{-1} (stratiform, 0.44 mm h^{-1}). During cruises 1 and 2 the TOGA radar data underrepresents the occurrence of echoes less than 20 dB*Z* and the corresponding very light rainfall rates. This discrepancy was due to different settings for Doppler thresholding of the reflectivity data in the two processors. On the basis of rain gauge measurements from Darwin, Australia, during the rainy season, it is estimated that such low rates represent less than 2% of total rainfall but up to 20% of rain occurrence (Short et al. 1993). Changes in the TOGA radar settings for cruise 3 resulted in a higher sensitivity to lower reflectivities but had a negligible effect on space–time averages of rainfall.

TABLE 4. Summary statistics of TOGA radar corrections listed in Table 3.

Correction	Amount of data affected (%)	Period of affected data in IOP	Average correction (dB*Z*)	Range of correction (dB*Z*)
C_1	100	All	< –2	0 to –8
C_2	6	Cruises 1 and 3	–2.3	–10 to +10
C_3	100	All	+3.4	–1.6 to +11
C_4	55	Largest corrections after 24 Dec in cruise 2, after 26 Jan in cruise 3	–0.7	–4.8 to +2.4

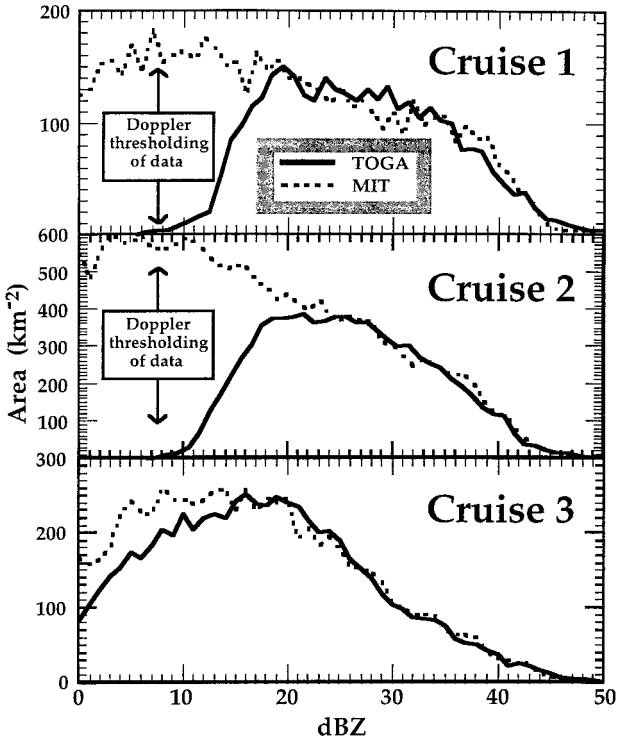

FIG. 3. Composite distributions of corrected radar reflectivity are compared between the TOGA and MIT radars for isolated echoes common to both radars at the same range (33 in cruise 1, 41 in cruise 2, and 22 in cruise 3).

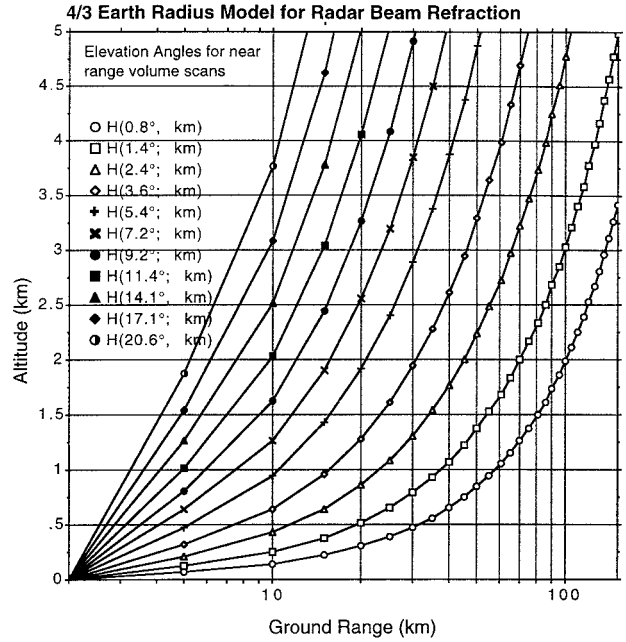

FIG. 4. Vertical cross section of the lowest 11 sweeps in a typical volume scan (4/3 earth model for atmospheric refraction).

3. Data processing and algorithms

The onboard processing and recording system provided digitized reflectivity values along with Doppler velocities and spectral width to a maximum range of 145 km (TOGA; 145–149 km MIT) during volume scans. Three different types of volume scans were available to the radar operators to maximize information content, depending on the range and intensity of echo patterns (see Kucera 1993). Figure 4 shows a vertical cross section of the 11 lowest tilts (out of 17 total) for a typical volume scan that was used when echoes were beyond 40-km range (the maximum elevation angle was 33°). To ensure detection of the tops of deep convective cells as they approached the radar, the maximum elevation was increased to 55° and the other 16 tilt angles adjusted to provide even volumetric coverage under those conditions. Ship motions prohibited routine scanning operations at elevations greater than 55°. In addition, to provide Doppler-derived divergence profiles under widespread stratiform conditions, an extended volume–azimuth display (see Srivastava et al. 1986) scan was included. It should be noted that these scans were usually executed intermittently as their elevation sequence resulted in rings of missing data in the hybrid Constant-altitude-plan-position indicators (CAPPIs). A surveillance scan consisting of three low-level elevation angles and having a maximum range of 295 km was also taken every 10 min.

From each volume scan, a polar coordinate reflectivity map near 2-km altitude was produced using a nearest neighbor sampling scheme. Once extracted from the full volume-scan dataset, these hybrid, CAPPI maps provided the basis for all subsequent calculations. The hybrid CAPPIs represent the reflectivity field near an altitude of 2 km, out to a range of 100 km. The altitude of the lowest elevation angle increases from 2 km at 100 km range to 3.8 km at 150 km range (see Fig. 4) due to earth curvature and refraction. Effects of this geometric property on rainfall measurements will be discussed in section 5.

Corrections for attenuation due to intervening rain (Jameson 1992), and a wet radome correction (Hudlow et al. 1979) based on readings from the optical rain gauges on the ships, were first applied to the polar CAPPIs data. The wet radome correction was not applied when the *PRC #5* was under way, due to vibration errors in the optical rain gauges (section 5). Because the *PRC #5* was under way only about 10% of the time and rain was observed during about 10%

of the time when under way, it is estimated that lack of a wet radome correction affects only 1% of the data.

Transformation to an initial convective rainfall rate using a conversion of $Z = 120\ R^{1.43}$ was performed in polar coordinates, after which averaging over a Cartesian 2 km × 2 km element was done by a high-resolution 8 × 8 averaging Cartesian grid within each Cartesian element (i.e., with 250-m resolution). This procedure weights the polar radar pixels in approximate proportion to their area, which increases as distance from the radar increases. The Cartesian grids from both ships were then merged using the maximum rainfall rate of either radar in the overlap area.

The convective *Z–R* relationship was based on analyses of raindrop size distribution data (DSD) observed on Kapingamarangi Atoll during the IOP (Tokay and Short 1996) and the vertical structure of convective echoes observed within the IFA by the shipboard radars (see section 4e; DeMott 1995). The surface-based DSD data gave indications of a systematic difference between convective and stratiform *Z–R* relationships, confirmed there and in Darwin, Australia, by comparisons of DSD data with vertical profiles of reflectivity from profilers and scanning radars (Tokay et al. 1995). For stratiform rainfall a relationship of $Z = 323\ R^{1.43}$ was adopted, resulting in stratiform rainfall rates being half as large as convective rainfall rates for the same reflectivity. A similar dual *Z–R* approach for rainfall estimation in midlatitudes is described in Table Z-2 of the Aviation Weather Services handbook (Aviation Weather Services 1995).

A simple convective/stratiform texture algorithm was applied to the initial Cartesian gridded rainfall rates, resulting in a convective core classification for grid points whose value exceeded the average of the surrounding 24 grid points (5 × 5 matrix) by a factor of 2 or more (see, e.g., Churchill and Houze 1984; Steiner et al. 1995). The eight grid points surrounding each core were also classified as convective. Also, all grid points with a rainfall rate exceeding 22 mm h^{-1} (40 dB*Z*) were classified as convective, in order to avoid misclassifying large contiguous areas of high rainfall rates as stratiform. All other points were then classified as stratiform and their rainfall rates were halved according to the *Z–R* relationships given above. The radar rainfall rates described above were then encoded logarithmically, using integer categories from 0 to 255, to provide a wide dynamic range of rainfall rates. The minimum rainfall rate encoded is 0.003 mm h^{-1}, while the maximum is 354.8 mm h^{-1}. The multiplicative factor between sequential rainfall rate categories is 1.047.

4. Rainfall patterns

The preexisting climatology suggests an annual rainfall of about 2500 mm (6.85 mm day^{-1}) within the IFA (Taylor 1973; Dorman and Bourke 1979; Elliot and Reed 1984), which lies between two rainfall maxima: the intertropical convergence zone north of the equator and the South Pacific convergence zone near 10°S. These analyses are based on extrapolation of island-based measurements or ship reports, which are sparse in the region. Analyses of satellite data and other meteorological fields (Gutzler et al. 1994) indicate that the TOGA COARE area experiences the following: 1) a distinct annual cycle (Meehl 1987); 2) considerable intraseasonal variability associated with low-frequency oscillations, such as the 40–60-day Madden–Julian oscillation (Lau and Chan 1985; Madden 1986; Nakazawa 1995); and 3) occasional westerly wind bursts sometimes related to El Niño–Southern Oscillation (ENSO) events. Each of these factors affect cloudiness, rainfall, surface pressure, wind, and temperature. The warm phase of an ENSO event, as was observed during the IOP (Kousky 1994; Ding and Sumi 1995), usually results in a shift of active convection and warm surface waters from the western Pacific toward the east, especially near the equator (Rasmusson and Carpenter 1982).

a. Cruise 1

The first cruise, 10 November–10 December, had the least rainfall, as indicated by Table 5. In addition,

TABLE 5. Cruise averaged rainfall rates and convective/stratiform partitioning of total rainfall and areal coverage.

Statistic	Cruise 1	Cruise 2	Cruise 3	Average
Convective (%rainfall/%area)	80/34	71/26	72/26	74/29
Stratiform (%rainfall/%area)	20/66	29/74	28/74	26/71
Average rate (mm day^{-1})	3.4	6.6	3.8	4.8

cruise 1 had the highest percentage of convective rainfall (80%) and the highest percentage of convective occurrences (34%) as determined from all available radar rainfall pixels. The spatial pattern of mean rainfall during the period of dual-radar operations, 10–30 November, shown in Fig. 5, has the appearance of a small sample realization of a homogeneous, isotropic random field, suggestive of the predominance of small-scale convective cells and systems. A major large-scale event that occurred during the beginning of the cruise was the passage of a westward-propagating cloud disturbance, as indicated by infrared observations of cloudiness by Japan's Geostationary Meteorological Satellite (GMS) (TOGA COARE International Project Office, 1993), on 10–11 November (Mori 1995), in which the radar-observed convective features propagated eastward (see Veldon and Young 1994). This system passed through the radar coverage area in 12 h, producing a peak 12-h rainfall rate of 24 mm day^{-1} (Fig. 6). Figure 6 also shows a major pulse of rainfall on 23–24 November (8.2 mm day^{-1} for 2 days), which was also associated with a westward-propagating system.

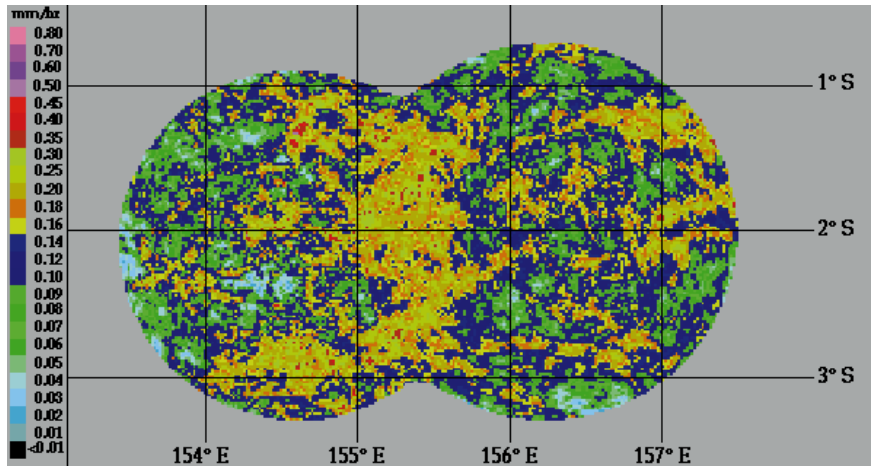

FIG. 5. Map of average rainfall rates for the time period of two-radar coverage, 10–30 November 1992. Intermittent coverage by the rain product extends beyond the area shown due to ship drift and repositioning legs. The pixels shown above had a > 50% occurrence of valid data.

b. Cruise 2

Cruise 2, 15 December–18 January, had significantly more precipitation than cruise 1, with maxima in the central and southern portion of the radar coverage area during the 3-week period of joint TOGA–MIT radar operations (22 December–9 January; Fig. 7). The early part of the cruise was the most active, associated with a major intraseasonal oscillation (as described by Nakazawa 1995) with two superclusters, strong westerly winds at the surface, and easterlies aloft. The second supercluster passage (20–25 December, IOP days 51–56) produced an average rainfall of 14.8 mm day^{-1}. This most active 2-week period of the IOP also produced an example of the quasi 2-day oscillation described by Takayabu (1994) and Takayabu et al. (1996), clearly evident in the radar rainfall time series (Fig. 8).

By the second half of cruise 2, conditions had returned to resemble those observed during most of cruise 1, with light winds and small, short-lived convective systems. The surface winds decreased and sea surface temperatures increased during this period (Sui et al. 1997).

c. Cruise 3

The average rainfall pattern for cruise 3 shows a pronounced NE–SW gradient with the highest values to the east (Fig. 9). This pattern was produced by a mixture of small isolated convection and large-scale systems. During late January, a second intraseasonal oscillation occurred with two superclusters (Nakazawa

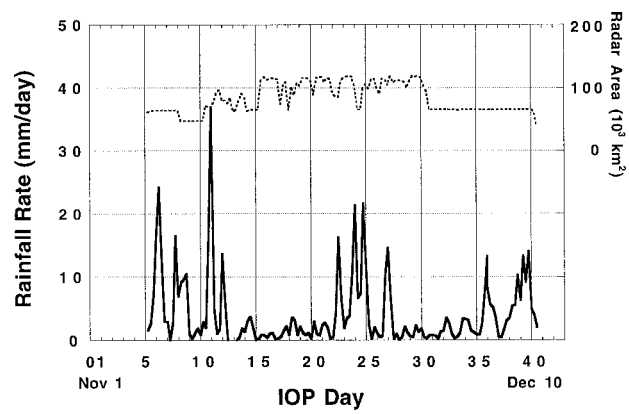

FIG. 6. Time series of area-average rainfall rates (mm day^{-1}) and radar coverage area (10^3 km^2), for 6-h intervals using all available radar data, for the time period 10 November–10 December 1992. Single radar coverage is evident at the beginning and end of the cruise. The local minimum of radar coverage ending around 10 November is due to a trial interlude of scans with a maximum 125-km range on the TOGA radar.

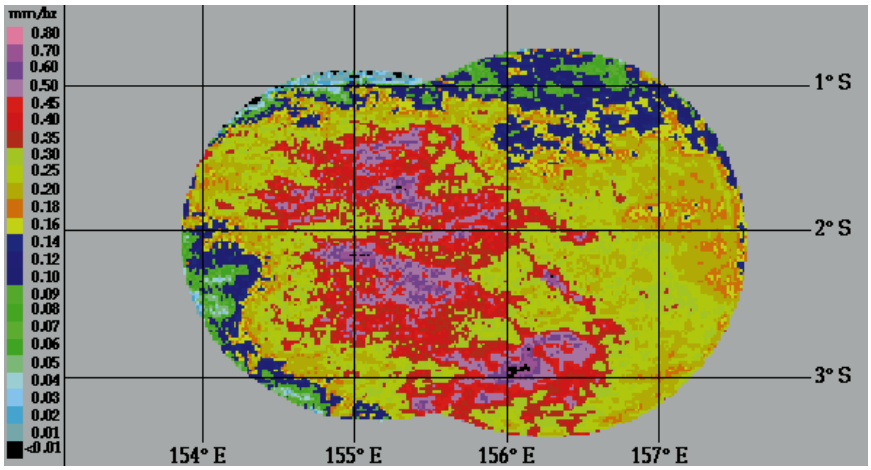

FIG. 7. Same as Fig. 5 but for the period 21 December 1992–10 January 1993.

1995). Some indications of the quasi-2-day wave are evident during IOP days 89–94 and 101–113 (Fig. 10). Also notable is a pronounced dry period from 2 to 9 February (IOP days 94–111), coinciding with the presence of Tropical Cyclone Oliver 1500 km to the south (TOGA COARE International Project Office 1993).

d. Convective/stratiform rainfall

Because rainfall within the IFA was largely initiated by convective processes, transitions from convective to stratiform rainfall (Zipser 1969; Houze 1981), such as that shown in Fig. 11, were common. Viewing of animated loops of the radar rainmaps indicated that some convective/stratiform sequences were due to propagation of systems through the radar array, especially squall lines with regions of trailing stratiform rain, whereas at other times there were clear indications of decaying convection transforming to stratiform with minimal propagation. During the major active period from 20 to 25 December, total rainfall was 61% convective and 39% stratiform. During cruise 1 the few major rain-producing systems were 68% convective, 32% stratiform, while inactive periods with isolated convection resulted in rainfall totals that were 85% convective and 15% stratiform. Overall, during disturbed periods defined by GMS infrared brightness temperature patterns within the IFA and animated sequences of the rainmaps (Sui et al. 1997), 70% of the total rainfall was convective (30% stratiform), whereas 88% of the total rain was convective (12% stratiform) during inactive periods.

The convective/stratiform maps generated in this study can be considered as an initial estimate, due to the simple nature of the discrimination algorithm. Nevertheless, validation of the texture algorithm is provided in Fig. 12, which shows the average radar reflectivity profiles from 1- to 6-km altitude for convective rainfall rates of 4, 8, 16, 32, 64, and 128 mm h^{-1}, and for stratiform rainfall rates of 1, 2, and 4 mm h^{-1}. Note that the stratiform profiles have a local maximum at 4.5 km due to the presence of the radar "bright band," whereas the convective profiles lack such a feature. Steiner et al. (1995) have indicated that convective/stratiform classification algorithms based on horizontal texture are sensitive to the spatial resolution of the gridded radar data and should be "tuned" to specific environments. Testing of alternative algorithms (DeMott 1995; Rosenfeld et al. 1995) is beyond the scope of the present study.

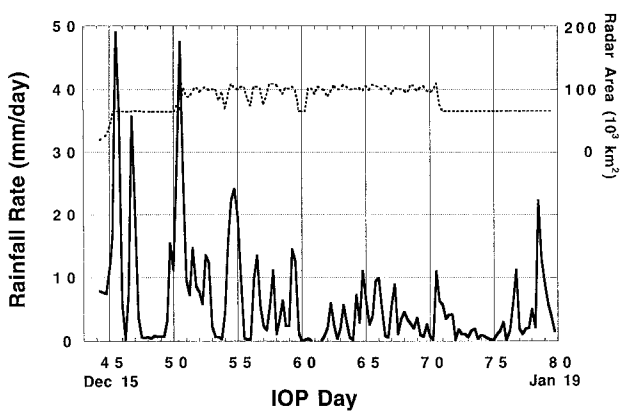

FIG. 8. Same as Fig. 6 but for the period 14 December 1992–19 January 1993.

e. Diurnal variations

Figure 13 shows the mean diurnal cycle for total, convective, and stratiform rainfall for 94 days of radar data. The maximum rainfall occurred just after midnight and the minimum just before noon, local time. The convective sequence shows a peak just after midnight, in phase with the peak in total rainfall. These results differ somewhat from those of Hendon and Woodberry (1993), who analyzed an index of deep convective activity (DCA) derived from satellite infrared observations and found that it maximized between 0600 and 0900 over the oceans throughout the Tropics. The discrepancy between their global

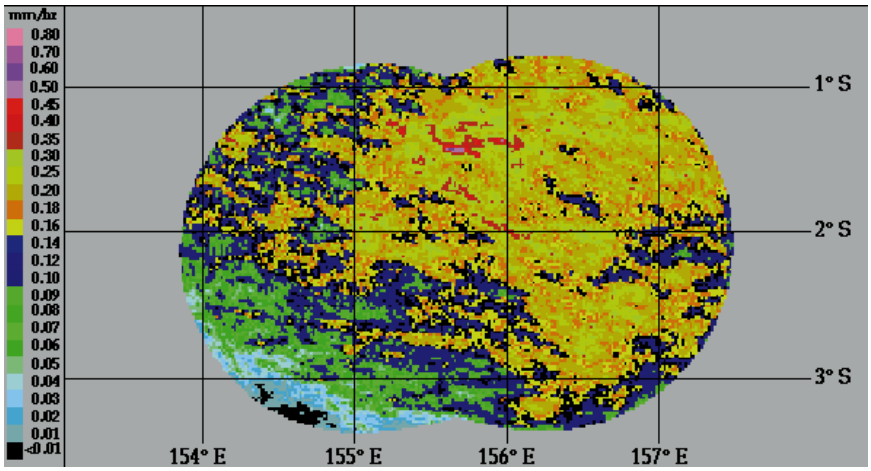

FIG. 9. Same as Fig. 5 but for the period 29 January–19 February 1993.

analysis, based on almost 1 yr of satellite data, and the present local analysis, based on less than 4 months of radar data, could be resolved by a combined analysis of their DCA index, calculated from GMS IR data, and the TOGA COARE radar rainfall product.

Figure 13 also shows an indication of a weak secondary peak in the early afternoon, in phase with the diurnal peak in sea surface temperature (Sui et al. 1997). In their independent analysis of the present radar rainfall product, Sui et al. (1997) identified an early afternoon maximum in widely scattered rain showers during conditions when the large-scale environment was undisturbed and the scattered showers failed to organize into mesoscale systems. It is unlikely that such widely scattered showers would influence an IR-based index of deep convective activity such as that used by Hendon and Woodberry (1993).

The stratiform sequence in Fig. 13 shows a peak in the early morning hours, several hours after the peak in convective and total rainfall. This indication of a convective/stratiform sequence during the diurnal cycle was also noted by Hendon and Woodberry (1993) and is consistent with the general life cycle of convectively induced tropical precipitation (Houze and Betts 1981).

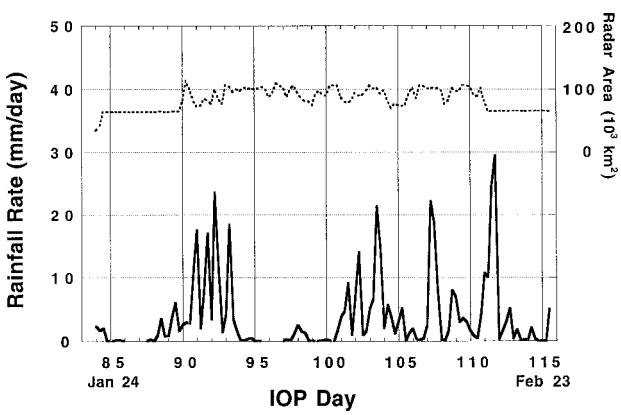

FIG. 10. Same as Fig. 6 but for the period 23 January–20 February 1993.

f. *Vertical structure and range dependence*

The vertical structure of precipitating clouds can cause errors in radar estimates of rainfall. For example, the mean reflectivity profile in Global Atmospheric Research Program (GARP) Atlantic Tropical Experiment (GATE) and TOGA COARE convective cells showed a decrease of about 0.5 dBZ km^{-1} at low levels, and a more rapid decrease of 1 dBZ km^{-1} or more above the 0°C level [see Fig. 12, Szoke et al. (1986); DeMott (1995)]. This suggests that surface convective rainfall derived from reflectivity measurements aloft will be systematically underestimated, unless some compensation is made for the vertical structure. The vertical structure for convective precipitation, combined with the horizontal scale of rain cells and the conical nature of the radar beam will introduce a complex range dependence, leading to underestimates of rainfall at far ranges (Rosenfeld et al. 1992). On the other hand, tropical stratiform rain falls from

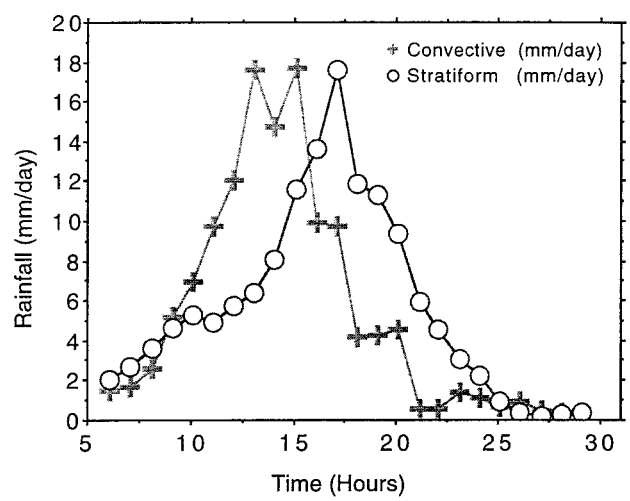

FIG. 11. Time series of area-averaged convective and stratiform rainfall observed within the IFA on 22–23 December 1992. Total rainfall for this event was 48% convective, 52% stratiform.

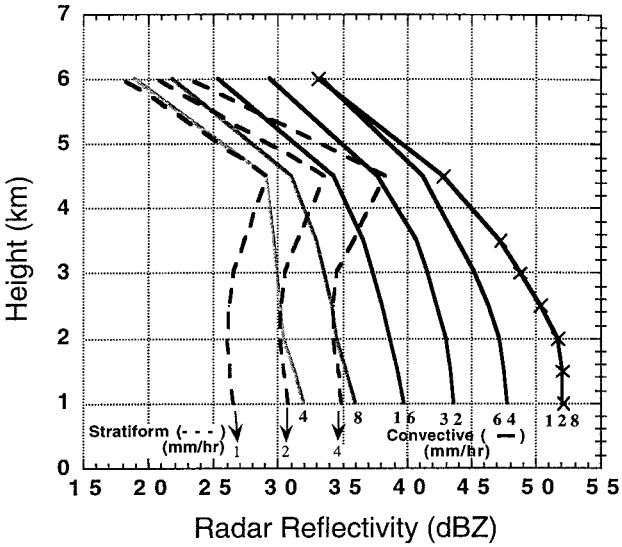

FIG. 12. Average radar reflectivity profiles from 1- to 6-km altitude for stratiform rainfall rates of 1 (33 742), 2 (24 013), and 4 (10 813) mm h^{-1} and convective rainfall rates of 4 (10 145), 8 (10 122), 16 (9078), 32 (4909), 64 (1034), and 128 (179) mm h^{-1}. Numbers in parentheses indicate the number of profiles used in computing the mean. Profiles were observed within 60 km of the radars.

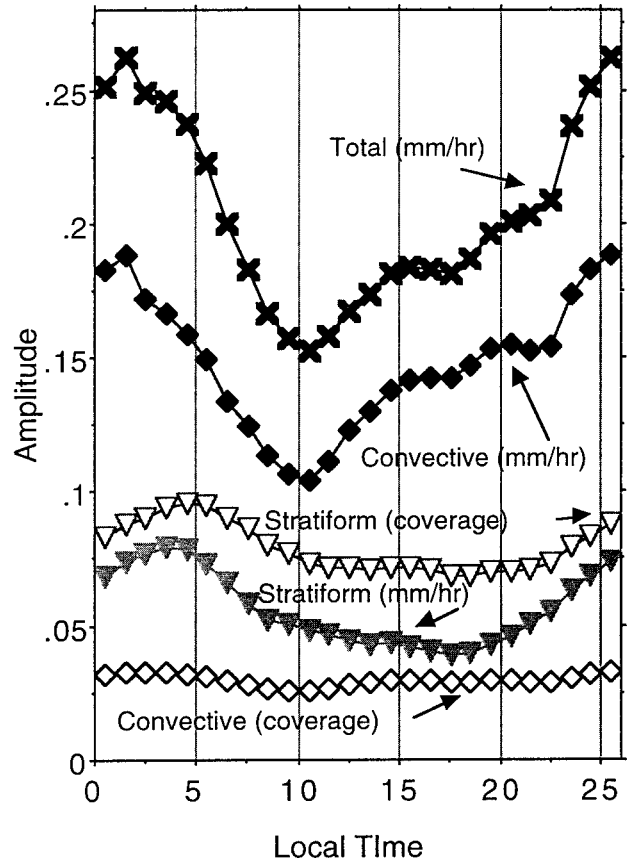

FIG. 13. Diurnal variation of average rainfall rate (x), convective rainfall rate (closed diamonds), fractional coverage by stratiform rain (open triangles), stratiform rainfall rate (closed triangles), and fractional coverage by convective rain (open diamonds).

a layer of melting aggregates, which constitute the well-known radar bright band, a region of enhanced reflectivity just below the 0°C isotherm. Stratiform conditions can lead to an overestimation of rainfall rate at the range where the radar beam intercepts the bright band (Smith 1986). Since the 0°C isotherm in the TOGA COARE region was typically at a height of about 5 km, the radar bright band is expected between 4 and 5 km. Figure 2 indicates that the center of the radar beam, for an elevation of 0.8°, would intercept the 4.5-km level at a range beyond 150 km. However, because of the 1.55 beamwidth of the radars deployed during TOGA COARE, the upper portion of the radar beam (defined by the "half-power point") intercepts this sensitive zone at a range of 135 km. Thus, vertical structure can introduce a complex mean-error structure into radar rainfall measurements.

An analysis of the area-averaged vertical structure of precipitation was made over the 60-km radius circle surrounding each radar. A sequence of CAPPIs were made at altitudes from 1 to 6 km (1, 1.5, 2, 2.5, 3, 3.5, 4.5, and 6; see Fig. 14). For each CAPPI, an area-averaged rainfall rate was retrieved at each level using a convective Z–R relation. Figure 14 shows the average profile, normalized with respect to the value at 2-km altitude. This profile represents average conditions over a mesoscale-sized area (11 310 km^2), showing that rainfall rates inferred from reflectivity measurements at 2-km altitude will, on average, be less than at 1 km. By projecting the shape of the average profile to the surface, it is estimated that average radar–rainfall rates at the 2-km level will tend to underestimate surface rainfall rates by approximately 11%. To compensate for this average vertical structure, the surface-based convective Z–R from Tokay and Short (1996) was modified to increase rainfall by 11% (0.45 dBR). Techniques being developed to compensate for vertical structure effects in each scan and at each location (Andrieu and Creutin 1995) were not implemented for these products because of the complex iteration that results between vertical structure corrections, attenuation corrections, convective/stratiform classification, and Z–R selection.

Vertical structure in the reflectivity field will also result in a range dependence in the rainfall products beyond 100-km range. Note that the altitude of the lowest elevation angle increases from 2 km at a range

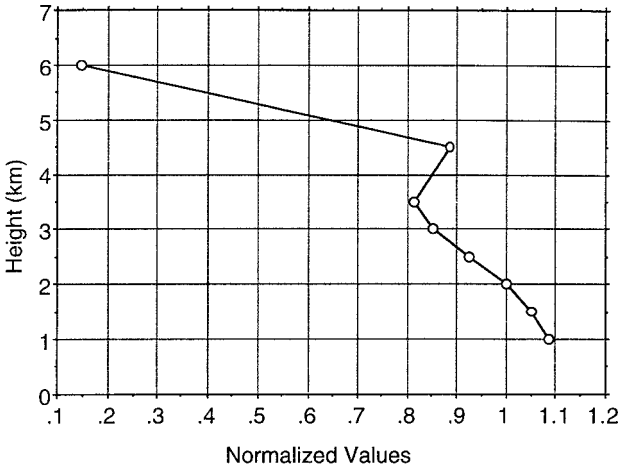

FIG. 14. Vertical profiles of area-averaged rainfall rate, normalized with respect to the value at 2-km altitude, for the area within 60 km of the radar. The average profile (x) shows a 9% increase from 2 to 1 km.

of 100 km to 3.5 km at 150-km range (Fig. 4). The mean profile in Fig. 14 shows a decrease of 16% from 2 to 3.5 km, suggesting a range dependence with a decrease of that magnitude, due to vertical structure alone, in the outer 50-km range of the rainmap product.

An objective determination of range dependence was made by examining TOGA and MIT radar data along the baseline between the two radars. For example, with a baseline of 150 km, rainfall rates within 50 km of the TOGA radar were systematically higher than corresponding rates occurring at a range of 100–150 km from the MIT radar. The opposite was found for rates within 50 km of the MIT radar. A clear indication of range dependence was evident for both radars, approaching a 50% underestimation at a range of 150 km. As a further test of range dependence the circular area of coverage for each radar was divided into nine equal-area annuli with boundaries as listed in Table 6. A special unmerged rainmap was made for each radar, and rainfall totals were determined for each annulus, each radar, and each cruise. This analysis revealed an overall range dependence similar to the baseline analysis, with variations from cruise-to-cruise due to varying meteorological patterns. The effect of east–west gradients in the rain fields was also determined by examining range-dependent statistics for the eastern and western halves of each radar separately. There was some indication of a weaker range dependence in the MIT radar data, partly ascribable to differences in Doppler coherence thresholding of data between the two radars (see Fig. 3 and Ferrier et al. 1995a), and partly due to weaker east–west gradients in the eastern half of the IFA where the MIT radar was stationed.

On the basis of the baseline analysis and examination of the azimuthally averaged fields, a range-dependent correction was determined for the version 2 product. Table 6 lists recommended gain factors and equivalent dBZ adjustments for the unmerged product. Application of the gain factors to the version 2 product will increase overall rainfall by 12% from 4.8 to 5.4 mm day^{-1}. Note that for the products merged from both radars, the gain should be applied outside the area of overlap between the two radars (in the overlap area the highest rainfall rate was used). Also, it is important to note that these corrections are for the average rainfall fields and will tend to overcorrect stratiform rain and undercorrect convective rain.

5. Radar-optical rain gauge comparisons

During the TOGA COARE IOP optical rain gauges (ORGs) were deployed on six buoys, 13 research vessels, one atoll (Wilkerson 1994), and one island (Suzuki 1994). The ORG senses rainfall rate through fluctuations in the intensity of an infrared beam caused by raindrops falling between the transmitter and a single, slotted receiver. The transmitter and receiver are separated by about 50 cm (Nystuen and Proni

TABLE 6. Recommended range-dependent gain factors applicable to the average rainfall field.

Range interval (km)	Gain factor	Equivalent dBZ
0.000–50.000	1.000	0.000
50.000–70.711	1.000	0.000
70.711–86.603	1.000	0.000
86.603–100.000	1.000	0.000
100.000–111.803	1.038	0.231
111.803–122.474	1.126	0.739
122.474–132.289	1.247	1.372
132.289–141.425	1.393	2.060
141.425–150.000	1.560	2.760

1996). The fluctuating signal is bandpass filtered and transformed to rainfall rate via an algorithm designed under the assumption that the raindrop size distribution is exponential. The majority of these gauges were calibrated in natural rain on land where reliable performance was observed, although a sensor-dependent gain adjustment was evident. A full assessment of performance aboard the mobile platforms in TOGA COARE is incomplete at this time; however, preliminary indications are that the ORGs tended to overestimate rainfall and were susceptible to effects of vibration, which causes spurious peaks in rainrate records from individual ORGs (Short et al. 1994).

a. Direct comparisons

Of the 21 platforms mentioned above, only the ATLAS mooring near 2°S, 156°E maintained a fixed station within range of the shipborne radars. Figure 15 shows variations in the platform position with respect to the 2×2 km grid of the radar rainfall product. The buoy was within 40 km of one radar or the other for a total of 99 days. Table 7 lists some statistics of radar and ORG rainfall observed at the site. The ORG indicates 2.53 times more rain than the radar. However, the radar indicates only about 14% more hours of rainfall rates greater than 0.5 mm h^{-1}, the minimum detectable signal for the ORG. Thus, the discrepancy between the two is largely due to differences in the average rainfall rate, when raining. The overall correlation between the radar and buoy daily rainfall totals was found to be 0.77. The correlation was maximum during cruise 2 (0.88) and minimum during cruise 3 (0.56), due to reasons given in the paragraph below. Table 7 shows that the average rainfall rate, when raining, differs by a factor of 3.02 between the buoy ORG and the collocated radar rainfall data. Rainfall rates below 0.5 mm h^{-1} contribute about 5% of the total radar rainfall (see Table 5 footnote). If it is assumed that the ORG rainfall total is low by 5%, due to the minimum detectable rate of 0.5 mm h^{-1}, the ratio between radar and ORG total rainfall becomes 2.65 [(1.05) 1416/560]. If it were further assumed that the radar totals were low due to a calibration offset, a correction of 6 dBZ would be required to make up the discrepancy. Such a large correction to the radar data cannot be justified on the basis of the extensive calibrations performed before, during, and after the TOGA COARE field experiment. Furthermore, a study of conditional rainfall rate statistics from the TOGA COARE buoy ORGs with those from rain gauges on western Pacific islands and atolls (Morrissey et al. 1994) suggests that when it is raining, the ORG rates are 2–3 times greater than those from the islands and atolls, consistent with the direct ORG–radar comparison discussed above.

Some differences are expected between the radar and ORG measurements because of the mismatch in scale (point vs area average); however, average radar rainfall rates in adjacent grid elements are not highly

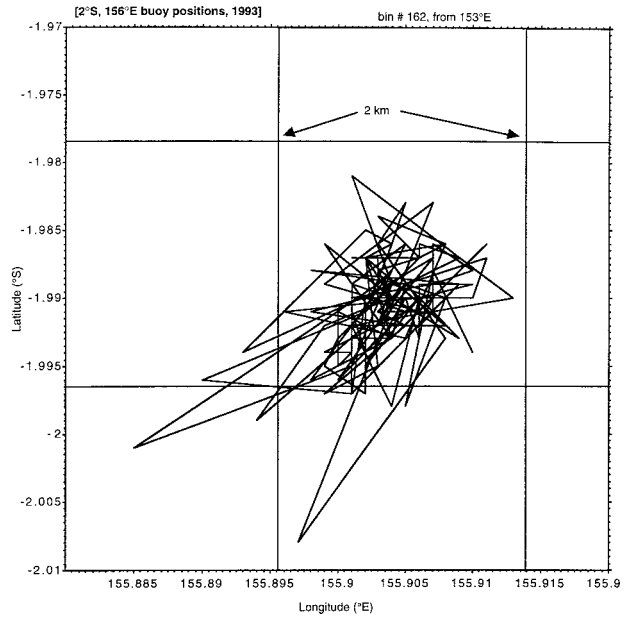

FIG. 15. Position variation of Atlas mooring near 2°S, 156°E within the radar rainfall grid during the COARE IOP.

TABLE 7. Radar and optical rain gauge statistics at the 2°S, 156°E ATLAS mooring site during 99 days of the COARE IOP.

Statistic	Device	
	Radar	Optical rain gauge
Rainfall (mm)	560 (5.7 mm day^{-1})	1416 (14.3 mm day^{-1})
T (h) > 0.0 mm h^{-1}	255.3	102.5
T > 0.5 mm h^{-1}	116.4	102.5**
Conditional (mm h^{-1})	4.57*	13.81

*95% of total rainfall occurred at rates > 0.5 mm h^{-1}.
**ORG minimum detectable rate is 0.5 mm h^{-1}.

variable, as shown in Fig. 16, suggesting that extreme spatial gradients in the mean field are not responsible for the discrepancy. The greatest difference between buoy and radar daily totals (15 vs 125 mm) occurred on 28 January 1993 when widespread rains hit the single radar ship on station (the *PRC #5*) and the buoy at the same time (1300–1500 UTC). The radar log indicates a sequence of special Doppler volume scans for estimating the local vertical profile of divergence, at the expense of contiguous coverage over an annulus containing the buoy location. It is also possible that the wet radome attenuation correction was insufficient in this case.

Preliminary comparisons between radar and ORG rainfall from shipboard ORGs have been accomplished by "navigating" the ships through the radar rainfall grid. The grid element containing the ship's position was determined and an $N \times N$ subset centered on that element was extracted (Bradley et al. 1996). The largest amount of data available for this type of comparison is from R/V *Moana Wave*, which maintained station near 1°45′S, 156°E during three separate cruises. Radar rainfall observations over the *Moana Wave* are available for 42 days, during which time the radar reported an average rate of 5.52 mm day^{-1}, whereas the ORG reported 13.82 mm day^{-1} for the same days, 2.5 times more than the radar. Correlation of the daily time series is 0.78. During the 42-day period the ORG reported 85.8 h of rainfall, while the radar reported only 54.7 h over the ship position. The discrepancy in frequency of occurrence of rainfall is much greater than that between the radar and buoy ORG, suggesting that ship vibrations may have affected ORG performance on the *Moana Wave*. At the present time the large discrepancies in rainfall indicated by the ORGs on the R/V *Moana Wave* and the 2°S, 156°E ATLAS mooring, and the radar rainfall over the same areas are not well understood.

5.9	5.7	5.7	7.0	6.4
6.0	6.2	6.0	6.2	6.5
5.7	5.3	5.7 14.3 (ORG)	5.8	5.9
5.9	5.6	5.8	5.6	5.8
5.5	5.5	5.9	5.8	6.2

FIG. 16. Mean radar rainfall rates (mm day^{-1}) over the Atlas mooring position and surrounding 2 km × 2 km grid elements for 99 days of the TOGA COARE IOP. Included is the rate for the optical rain gauge for the same 99 days.

Short et al. (1994) reported on random spikes of high rainfall rates (> 20 mm h^{-1}) observed in high-resolution times series of ORG rainfall that occurred as the *PRC #5* got under way during a rainstorm. The spikes persisted for about an hour as the ship repositioned through a background of light rain (< 5 mm h^{-1}). Table 8 shows that overall, the ORGs aboard the *PRC #5* recorded substantially higher rainfall rates when the ship was under way as compared to those observed while drifting. Although the underway sample size is small, by assuming a decorrelation time of 5 min and 54 independent samples, the difference in means appears to be statistically significant.

b. An indirect comparison

Because of the difficulties in obtaining absolute validation of radar rainfall measurements over the open ocean, an indirect comparison of rainfall statistics from ORG data and from the radar rainfall product was made. As noted above, ORG performance on the *PRC #5* was more reliable when the ship was drifting (speed < 2 m s^{-1}). A total of 44 days of ORG data was available under those conditions during cruises 2 and 3. A statistical comparison of ORG rainfall with radar rainfall grids within 3–7 km of the ship were analyzed for this "drifting" subset.

To compare the ORG point measurements with spatially averaged radar rainfall, an appropriate timescale for averaging the point data should be selected. Following Zawadzki (1975), ORG data were

TABLE 8. Comparison of optical rain gauge statistics observed on board the R/V *Xiang Yang Hong #5* during rainfall > 0.5 mm h^{-1} while the ship was drifting vs under way.

Statistic	Condition	
	Drifting	Under way
Mean (mm h^{-1})	6.4	16.4
Standard deviation (mm h^{-1})	14.2	30.2
Hours	73.9	4.5

time averaged to 1-, 4-, and 8-min resolutions from their original 1-s sampling to approximate the statistics to be expected from 2 km × 2 km area averages assuming raincell propagation rates of 43.3, 10.8, and 5.4 m s^{-1}. Table 9 indicates that while the ship was drifting, the ORG recorded about 6.5 mm day^{-1} of rainfall, whereas the percent occurrence of rainfall rate > 0.5 mm h^{-1} increased from 5.1% to 6.0% as the time averaging increased from 1 to 8 min, and the average rainfall rate, when raining decreased from 5.27 to 4.49 mm h^{-1}.

During the 44 1/3 days of drift the composited radar rainfall field within 3–7 km of the ship indicated a total rainfall of 7.06 mm day^{-1}, with a 12.3% occurrence of rain. However, when the radar statistics are truncated at 0.5 mm h^{-1} to match the ORG minimum detectable signal, the rainfall decreases by a factor of 0.944 to 6.67 mm day^{-1}, while the occurrence decreases to 6.1%. As a further illustration of the overall agreement between the radar and ORG statistics, Fig. 17 shows matched percentiles of the ORG and radar cumulative rainfall rate distributions for the 8-min ORG data. There is excellent agreement over a range of rainfall rates from 0.5 to 60 mm h^{-1}. This indicates that the ORG and radar rainfall rate distributions are quite similar over that range.

TABLE 9. Statistics of ORG rainfall rates (for $R > 0.5$ mm h^{-1}) vs averaging time for 44 1/3 days of drifting during cruises 2 and 3.

Statistic	Period		
	1 min	4 min	8 min
Hours	54.58	59.42	63.60
Mean (mm h^{-1})	5.27	4.83	4.49
Std dev (mm h^{-1})	10.62	9.14	7.65
Rate (mm day^{-1})	6.49	6.48	6.45
Occurrence	5.1%	5.6%	6.0%

6. Discussion of radar comparisons and uncertainties

As a first step toward establishing realistic estimates of rainfall accuracy and the calibration stability of the two radars, a statistical comparison was made of area-averaged rainfall rate (AARR) from each radar in the region of overlap. As discussed in section 2, periodic adjustments were made to the TOGA radar to bring the overall AARR from both radars into agreement. During their 64 days of joint operations during cruises 1, 2, and 3, average rainfall rates of 4.23 mm day^{-1} (MIT) and 4.11 mm day^{-1} (TOGA) were recorded in the region of overlap. Due to changes in assigned stations the average area of overlap increased from 14 000 km^2 in cruise 1, to 25 000 km^2 in cruise 2, to 30 000 km^2 in cruise 3. An overall bias of 3%, or 0.12 dBR [dBR = 10 Log_{10}(AARR)] is indicated for the MIT radar. During this same time interval, 99% of total rainfall accumulation was accounted for by only 4069 scans, representing less than half of the observations. A linear regression of these points in log–log coordinates results in a correlation of 0.928 and a root-mean-square (rms) error of 1.98 dBR. The high correlation indicates that "signals" due to meteorological variability during significant rainfall events are well represented by each system, with relatively small errors due to variations in radar performance ("noise").

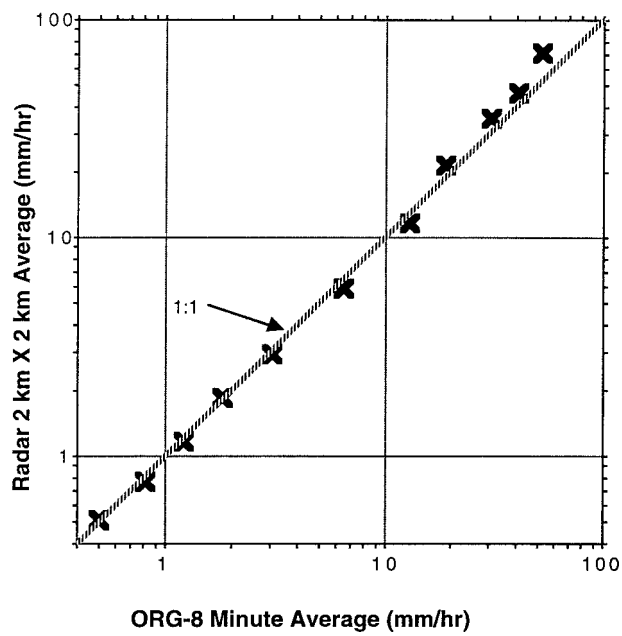

FIG. 17. Matched percentiles of rainfall rate distributions from the ORG #1 aboard the R/V *Xiang Yang Hong #5* and radar rainfall data from 2 km × 2 km pixels within 3–7 km of the ship while the ship was drifting. The temporal resolution of the ORG data is 8 min and both distributions are truncated at 0.5 mm h^{-1}. The percentiles begin at 0% (0.5 mm h^{-1}) and proceed in the following order: 16.7%, 33.3%, 50.0%, 66.7%, 83.3%, 91.7%, 95.8%, 98.3%, 99.2%, and 99.6%.

An estimate of the error can be obtained by computing the overall rms difference between the two radar estimates of AARR within the overlap region (following Chang et al. 1993). They have shown that the effective error is found by dividing the rms error by $2^{1/2}$, resulting in an effective rms error of 1.40 dB*R*. The effective rms error in dB*Z*, found by multiplying by 1.43, the power coefficient in the *Z–R* relation, is 2.00 dB*Z*. Table 10 shows the rms error (dB*R*), effective rms error (dB*R*), and effective rms error (dB*Z*) for instantaneous, 6-h, and daily averages of rainfall within the overlapping radar area (typically 25 000 km^2).

It is likely that the radar performance was better than indicated in Table 10, when interpreted in terms of stability and calibration. This is because measurements in the large overlap area will be affected by all possible configurations of echoes and echo structure, introducing errors due to uncompensated attenuation, range dependence, and vertical structure into the comparison. As a result, it can be concluded that for individual volume scans the radars were stable to better than 2 dB*Z*, while their daily averaged stability was better than 1 dB*Z*.

The methods used to estimate rainfall rate from reflectivity measurements can also be considered as a source of uncertainty, due to the complex relationship between the radar observable and the rainfall rate at the surface. As an example, consider the dual *Z–R* method used in the present study. It differs slightly from Tokay and Short's (1996) analysis of raindrop size distribution data from Kapingamarangi Atoll. Their results suggest that for a given reflectivity, convective rainfall rates are higher by a factor that depends on *R* itself, ranging from 2.11 at 1 mm h^{-1} to 1.68 at 10 mm h^{-1}. The method adopted here uses a constant factor of 2, which is equivalent to a 4.3-dB*Z* difference in reflectivity, at the same rainfall rate. Use of the rainfall rate–dependent factor suggested above would have minimal impact on total rainfall and on the convective/stratiform apportionment, while at the same time introducing a nonreversible step in the data processing. Note that the effect of a single *Z–R* retrieval on the stratiform/convective rainfall ratio can be found by doubling all the stratiform rainfall rates. This would increase total rainfall by 26% and change the convective portion from 76% to 61%.

To test the sensitivity of the present product to variations in the *Z–R* relation, the form $Z = 230R^{1.25}$ [see Hudlow (1979); a description of the rainfall product from GATE] was applied to all the data. Overall rainfall decreased by 8%, while the correlation between area-averaged rainfall amounts for the individual rainmaps obtained from the two methods was 0.994. This result could be anticipated by considering the differences and similarities between the *Z* and *R* relations. It can be shown that the GATE relation intersects the present stratiform curve at a low reflectivity (13.3 dB*Z*) and the convective curve at a higher reflectivity (43.2 dB*Z*). Thus, in the vicinity of the intersections, the two approaches yield similar results. Because the range from 13.3 to 42.3 dB*Z* covers the majority of echoes that contribute to total rainfall, the two approaches yield similar overall rainfall totals. However, it should be noted that for reflectivity < 43.2 dB*Z* the present relation yields higher convective rainfall rates, whereas the GATE relation yields higher stratiform rainfall rates for reflectivities > 13.3 dB*Z*. As a result, it can be expected that the partitioning of total convective versus total stratiform rainfall will be affected by the two different approaches. For the GATE *Z–R* run total rainfall was 62% convective, 38% stratiform, an increase from the 26% contribution by stratiform rainfall using the dual *Z–R* approach.

The impact of different parameterized drop size distributions for convective and stratiform precipitation was assessed in a modeling study of GATE squall convection (Ferrier et al. 1995b). This was accomplished by assuming larger mean drop sizes consistent with 3-dB*Z* higher reflectivities in stratiform precipitation relative to convective rainfall of the same rate. The rates of rain evaporation in the stratiform region were much lower in runs where stratiform reflectivities were +3 dB*Z* than in runs where convective drop spectra were assumed throughout the storm, which yielded vertical profiles of radar reflectivity that compared

TABLE 10. Rms error of radar–radar comparison for the scans comprising 99% of total rainfall accumulation in the overlapping area, presented as a function of averaging period.

	Period		
Statistic	**Instantaneous**	**6-h average**	**Daily average**
Sample size	4070	157	48
Rms (dB*R*)	1.98	1.34	1.00
Effective rms (dB*R*)	1.40	0.95	0.71
Effective rms (dB*Z*)	2.00	1.35	1.01

much better with the observations. In numerical models the representation of rain evaporation, which is the dominant microphysical process below the melting layer in tropical stratiform clouds, is sensitive to the parameterized drop size distribution (Ferrier et al. 1995b; Swann 1996). In the context of the present study, a 3-dB*Z* difference would result in a factor of 1.62 difference in convective and stratiform rainfall rates, at the same reflectivity, increasing overall rainfall by 6% and the stratiform contribution from 26% to 30%.

7. Concluding remarks

Reflectivity observations from shipborne Doppler radars have been analyzed to derive patterns of rainfall within the IFA during the 4-month intensive observing period of TOGA COARE (November 1992–February 1993). Overall, the average rate observed was 4.8 mm day^{-1}, although application of an empirical, range-dependent correction factor would increase that total by about 12%. Extreme variations of rainfall were observed in both time and space in connection with large-scale events. During the most active 2-week period in late December, 9.9 mm day^{-1} was observed in connection with a westerly wind burst, an intraseasonal oscillation, and the passage of two superclusters with embedded quasi-2-day waves. Active periods were composed of sequences of individual events lasting 12–24 h yielding 20–30 mm day^{-1}, interspersed with rainfall minima near zero. The most suppressed week in early February showed 0.4 mm day^{-1}, following the active phase of a second intraseasonal oscillation and the development of Tropical Cyclone Oliver in the Coral Sea.

Convective/stratiform partitioning of rain type, accomplished by a simple texture algorithm, indicates that overall occurrence was dominated by stratiform, 71% to 29% convective, while total rainfall (mm) was primarily convective, 74% to 26% stratiform. However, during the most active periods the total rainfall partitioning was closer to 60% convective and 40% stratiform, while during inactive periods it was 85% convective and 15% stratiform. Time series of convective/stratiform partitioning, averaged over the radar area of 125 000 km^2, indicate a transition in the character of the rainfall from convective to stratiform during major and minor events.

The mean diurnal cycle indicates a rainfall maximum between 0100 and 0200, local time, predominantly convective, with a stratiform maximum a few hours later (0400–0500). The early morning maximum rainfall was most evident during major events, while a weak afternoon convective maximum was most evident during quiescent periods (Sui et al. 1997).

Comparison of radar rainfall with that observed by optical rain gauges (ORGs) aboard ships and buoys shows ORG rainfall to be higher by a factor of 2.5–3. When broken down into its component parts of frequency of occurrence and average rainfall rate when raining, the discrepancy reveals some differences between shipboard and buoy-mounted ORGs. Aboard ships the ORG appears to be influenced by ship vibrations, with a higher frequency of rain and a higher conditional mean. The ORG on the 2°S, 156°E mooring agreed well with the radar on frequency of occurrence but had a conditional mean rainfall rate three times higher. When viewed in comparison with rainfall statistics from nearby islands and atolls, the ORG statistics appear to be too high, while the radar statistics are more comparable.

Acknowledgments. The successful deployment of shipborne radars into the western equatorial Pacific for the 4-month TOGA COARE Intensive Observing Period and the collection of a high quality dataset required a dedicated effort of international dimensions, carried out by technicians, scientists, and managers, representing numerous countries, agencies, institutions, and areas of responsibility. The overall radar program was conducted under the direction of Chief Scientists O. W. Thiele (NASA/Goddard Space Flight Center; NOAA/TOGA radar) and S. A. Rutledge (Colorado State University; MIT radar). The R/V *Xiang Yang Hong #5*, from the State Oceanic Administration of the People's Republic of China, carried the NOAA/TOGA radar and the R/V *J. V. Vickers*, from the National Oceanic and Atmospheric Administration of the United States, carried the MIT radar. The captain and crew of both vessels provided outstanding support critical to the completion of the radar mission. The port facilities at Honiara, Solomon Islands, were utilized between cruises 1 and 2, and 2 and 3 for each ship for crew rest and personnel rotation. The coordination of these activities during field operations was made possible by the efforts of the COARE Operations Director, D. Carlson, the Honiara Operations Coordinator, G. Martin, and their staff.

Refurbishment, installation, at-sea maintenance, and calibration of the radars was accomplished by personnel from the NASA/Wallops Flight Facility (NOAA/TOGA radar; J. C. Gerlach, J. Pafford, P. Istvan) and the National Center for Atmospheric Research (MIT radar; J. Lutz, B. Bowie, M. Strong).

Round the clock operations during deployment in the Intensive Flux Array were carried out by personnel from NASA, Colorado State University, Texas Tech University, Texas A&M University, and the Massachusetts Institute of Technology, as follows.

NOAA/TOGA Radar (cruise 1: J. C. Gerlach, NASA; P. A. Kucera, Texas Tech University; cruise 2: D. A. Short, NASA; P. A. Kucera, Texas Tech University; and S. H. Veleva, Texas A&M

University; cruise 3: B. S. Ferrier, NASA; D. B. Wolff, NASA; and R. Barritt, Texas A&M University).

MIT Radar (cruise 1: C. A. Leary and A. L. Doggett, Texas Tech University; and C. A. DeMott, Colorado State University; cruise 2: G. M. Jurica and A. L. Doggett, Texas Tech University; and T. M. Rickenbach, Colorado State University; cruise 3: A. L. Doggett, Texas Tech University; R. Cifelli and W. Petersen, Colorado State University; and D. Bocippio, MIT).

Buoy rainfall and position data were supplied by M. McPhaden and L. Mangum (NOAA/PMEL).

References

Anderson, S. P., R. A. Wells, and R. Lukas, 1996: Surface buoyancy forcing and the mixed layer in the warm pool: Observations and one-dimensional model results. *J. Climate,* **9,** 3056–3085.

Andrieu, H., and J. D. Creutin, 1995: Identification of vertical profiles of radar reflectivity for hydrological applications using an inverse method. Part I: Formulation. *J. Appl. Meteor.,* **34,** 225–239.

Aonashi, K., A. Shibata, and G. Liu, 1996: An over-ocean precipitation retrieval using SSM/I multichannel brightness temperatures. *J. Meteor. Soc. Japan,* **74,** 617–637.

Austin, P. M., 1987: Relation between measured radar reflectivity and surface rainfall. *Mon. Wea. Rev.,* **115,** 1053–1070.

Aviation Weather Services, 1995: AC 00 - 45 D (a supplement to Aviation Weather AC 00 - 6A), 1995. Government Printing Office No. 050-007-01082-6, 124 pp. [Available from Government Printing Office, Washington, DC 20401.]

Bradley, E. F., and R. A. Weller, Eds., 1996: *Fourth Workshop of the TOGA COARE Air–Sea Interaction (Flux) Working Group.* Woods Hole Oceanographic Institution, 67 pp.

——, P. A. Coppin, P. A. Kucera, and D. A. Short, 1996: Comparisons of rainrate as measured by ship radars and by the optical raingauge on the R/V Franklin during TOGA-COARE. Preprints, *Second Int. Conf. on the Global Energy and Water Cycle,* Washington, DC, World Climate Research Program, 480–481.

Chang, A. T. C., L. S. Chiu, and T. T. Wilheit, 1993: Random errors of oceanic monthly rainfall derived from SSM/I using probability distribution functions. *Mon. Wea. Rev.,* **121,** 2351–2354.

Churchill, D. D., and R. A. Houze Jr., 1984: Development and structure of winter monsoon cloud clusters on 10 December 1978. *J. Atmos. Sci.,* **41,** 933–960.

Conley, R., 1993: GPS performance: What is normal? *Navigation: J. Inst. Navig.,* **40,** 261–281.

DeMott, C. A., 1995: An improved method for partitioning radar data into convective and stratiform components. *Proc. 27th Conf. on Radar Meteorology,* Vail, CO, Amer. Meteor. Soc., 233–236.

——, 1996: The vertical structure and modulation of TOGA COARE convection: A radar perspective. Ph.D. dissertation, Colorado State University, 160 pp.

Ding, Y. H., and A. Sumi, 1995: Large-scale atmospheric circulation features during TOGA COARE IOP. *J. Meteor. Soc. Japan,* **73,** 339–351.

Doggett, A. L., IV, 1996: Analysis of rainwater flux in the IFA during TOGA COARE using shipboard radar rainfall estimates. Ph.D. thesis, Texas Tech University, 174 pp.

Dorman, C. E., and R. H. Bourke, 1979: Precipitation over the Pacific Ocean, 30°S to 60°N. *Mon. Wea. Rev.,* **107,** 896–910.

Ebert, E. E., 1996: Results of the 3rd Algorithm Intercomparison Project of the Global Precipitation Climatology Product (GPCP). BMRC Research Rep. 55, 182 pp. [Available from Bureau of Meteorology Research Centre, GPO Box 1289, Melbourne, Victoria, Australia.]

——, M. J. Manton, P. A. Arkin, R. J. Allam, G. E. Holpin, and A. Gruber, 1997: Results from the GPCP Algorithm Intercomparison Programme. *Bull. Amer. Meteor. Soc.,* **77,** 2875–2887.

Ecklund, W. L., K. S. Gage, and C. R. Williams, 1995: Tropical precipitation studies using a 915 MHz wind profiler. *Radio Sci.,* **30,** 1055–1064.

Elliott, W. P., and R. K. Reed, 1984: A climatological estimate of precipitation for the world ocean. *J. Appl. Meteor.,* **23,** 434–439.

Esbensen, S. K., and M. J. McPhaden, 1996: Enhancement of tropical ocean evaporation and sensible heat flux by atmospheric mesoscale systems. *J. Climate,* **9,** 2307–2325.

Ferrier, B. S., J. Gerlach, P. Kucera, D. Short, S. Rutledge, J. Lutz, and O. Thiele, 1995a: Corrections and comparisons of TOGA COARE shipborne radar reflectivities. *Proc. 27th Conf. on Radar Meteorology,* Vail, CO, Amer. Meteor. Soc., 675–677.

——, W. K. Tao, and J. Simpson, 1995b: A double-moment multiple-phase four-class ice scheme. Part II: Simulations of convective storms in different large-scale environments and comparisons with other bulk parameterizations. *J. Atmos. Sci.,* **52,** 1001–1033.

Frank, W. M., and H. Wang, 1996: Rawinsonde budget analyses during the TOGA COARE IOP. *J. Atmos. Sci.,* **53,** 1761–1779.

Gage, K. S., C. R. Williams, and W. L. Ecklund, 1996: Application of the 915 MHz profiler for diagnosing and classifying tropical precipitating cloud systems. *Meteor. Atmos. Phys.,* **59,** 141–151.

Gosnell, R., C. W. Fairall, and P. J. Webster, 1995: The sensible heat flux of rainfall in the tropical ocean. *J. Geophys. Res.,* **100,** 18 437–18 442.

Gutzler, D. S., G. N. Kiladis, G. A. Meehl, K. M. Weickmann, and M. Wheeler, 1994: The global climate of December 1992–February 1993. Part III: Large-scale variability across the tropical western Pacific during TOGA COARE. *J. Climate,* **7,** 1606–1622.

Hendon, H. H., and K. Woodberry, 1993: The diurnal cycle of tropical convection. *J. Geophys. Res.,* **98,** 16 623–16 637.

Houze, R. A., Jr., 1981: Structures of atmospheric precipitation systems. *Radio Sci.,* **16,** 671–689.

——, and A. K. Betts, 1981: Convection in GATE. *Rev. Geophys. Space Phys.,* **19,** 541–576.

Hudlow, M. D., 1979: Mean rainfall patterns for the three phases of GATE. *J. Appl. Meteor.,* **18,** 1656–1669.

——, R. Arkell, V. Patterson, P. Pytlowany, and F. Richards, 1979: Calibration and intercomparison of the GATE C-band radars. NOAA Tech. Rep. EDIS 31, 98 pp. [Available from Government Printing Office, Washington, DC 20401.]

Jameson, A. R., 1992: The effect of temperature on attenuation-correction schemes in rain using polarization propagation differential phase shift. *J. Appl. Meteor.,* **31,** 1106–1118.

Kousky, V. E., 1994: A review of recent oceanic and atmospheric anomalies related to ENSO. *Proc. 19th Annual Climate Diagnostics Workshop,* College Park, MD, Climate Prediction Center, NCEP/NOAA, 1–4.

Kucera, P. A., 1993: Intercomparison of shipboard radars over the Pacific warm pool. M.S. thesis, Dept. of Geosciences, Texas Tech University, 190 pp.

——, and Coauthors, 1995: COARE IOP Rainfall from shipborne radars: 2: Analysis and comparison of gridded fields. *Proc. 27th Conf. on Radar Meteorology*, Vail, CO, Amer. Meteor. Soc., 681–683.

Lau, K. M., and P. H. Chan, 1985: Aspects of the 40–50-day oscillation during the northern winter as inferred from outgoing longwave radiation. *Mon. Wea. Rev.,* **113,** 1889–1909.

Lin, X., 1997: Multiscale variability associated with the intraseasonal oscillation over the western Pacific warm pool. Ph.D. dissertation, Colorado State University.

——, and R. H. Johnson, 1996: Heating, moistening, and rainfall over the western Pacific warm pool during TOGA COARE. *J. Atmos. Sci.,* **53,** 3367–3383.

Madden, R. A., 1986: Seasonal variations of the 40–50-day oscillation in the tropics. *J. Atmos. Sci.,* **43,** 3138–3158.

Masters, J. M., and J. A. Leise, 1993: Correction of inertial navigation with Loran C on NOAA's P-3 aircraft. *J. Atmos. Oceanic Technol.,* **10,** 145–154.

Meehl, G. A., 1987: The annual cycle and interannual variability in the tropical Pacific and Indian Ocean regions. *Mon. Wea. Rev.,* **115,** 27–50.

Mori, K., 1995: Equatorial convection observed by the research vessel *Keifu Maru* during the TOGA COARE IOP, November 1992. *J. Meteor. Soc. Japan,* **73,** 491–508.

Morrissey, M. L., W. F. Krajewski, and M. J. McPhaden, 1994: Estimating rainfall in the Tropics using the fractional time raining. *J. Appl. Meteor.,* **33,** 387–393.

Nakazawa, T., 1995: Intraseasonal oscillations during the TOGA COARE IOP. *J. Meteor. Soc. Japan,* **73,** 305–319.

Nystuen, J. A., and J. R. Proni, 1996: A comparison of automatic rain gauges. *J. Atmos. Oceanic Technol.,* **13,** 62–73.

Oki, R., P. A. Kucera, and D. A. Short, 1997: Triple shipborne observations of tropical mesoscale convective systems during TOGA COARE. *Proc. 22nd Conf. on Hurricanes and Tropical Meteorology*, Fort Collins, CO, Amer. Meteor. Soc., 323–324.

Parsons, D., and Coauthors, 1994: The integrated sounding system: Description and preliminary observations from TOGA COARE. *Bull. Amer. Meteor. Soc.,* **75,** 553–567.

Petersen, W. A., S. A. Rutledge, and R. E. Orville, 1996: Cloud-to-ground lightning observations in TOGA COARE: Lightning location algorithms and selected results. *Mon. Wea. Rev.,* **124,** 602–620.

Polyak, I., G. R. North, P. A. Kucera, and N. R. Smith, 1997: Variability of the Tropical Ocean Global Atmosphere Coupled Ocean–Atmosphere Response Experiment rain rate observations. *J. Geophys. Res.,* **102,** 11 103–11 111.

Rasmusson, E. M., and T. H. Carpenter, 1982: Variations in tropical sea surface temperature and surface wind fields associated with the Southern Oscillation/El Nino. *Mon. Wea. Rev.,* **110,** 354–384.

Rosenfeld, D., D. Atlas, D. B. Wolff, and E. Amitai, 1992: Beamwidth effects on *Z–R* relations and area-integrated rainfall. *J. Appl. Meteor.,* **31,** 454–464.

——, E. Amitai, and D. B. Wolff, 1995: Classification of rain regimes by the three-dimensional properties of reflectivity fields. *J. Appl. Meteor.,* **34,** 198–211.

Sauvageot, H., 1994: Radar measurement by radar: A review. *Atmos. Res.,* **35,** 27–54.

Short, D. A., D. B. Wolff, D. Rosenfeld, and D. Atlas, 1993: A study of the threshold method utilizing rain gauge data. *J. Appl. Meteor.,* **32,** 1379–1387.

——, O. W. Thiele, and M. J. McPhaden, Eds., 1994: *Optical Rain Gauge Performance, Second Workshop on Optical Rain Gauge Measurements*. NASA Conf. Publ., 76 pp.

——, P. A. Kucera, B. S. Ferrier, and O. W. Thiele, 1995: COARE IOP rainfall from shipborne radars: 1. Rainmapping algorithms. *Proc. 27th Conf. on Radar Meteorology,* Vail, CO, Amer. Meteor. Soc., 678–680.

Smith, C. J., 1986: The reduction of errors caused by bright bands in quantitative rainfall measurements made using radar. *J. Atmos. Oceanic Technol.,* **3,** 129–141.

Srivastava, R. C., T. J. Matejka, and T. J. Lorello, 1986: Doppler radar study of the trailing anvil region associated with a squall line. *J. Atmos. Sci.,* **43,** 356–377.

Steiner, M., R. A. Houze Jr., and S. E. Yuter, 1995: Climatological characterization of three-dimensional storm structure from operational radar and rain gauge data. *J. Appl. Meteor.,* **34,** 1978–2007.

Sui, C.-H., K.-M. Lau, Y. Takayabu, and D. A. Short, 1997: Diurnal variations in tropical oceanic cumulus convection during TOGA COARE. *J. Atmos. Sci.,* **54,** 639–655.

Suzuki, T., D. Abe, and K. Takeuchi, 1994: Note: The validity of optical precipitation sensor on the tropical ocean. Institute of Low Temperature Science Report, Hokkaido University, 12 pp. [Available from Institute of Low Temperature Sci-ence, University of Hokkaido, 8-5 Kita-ku, Sapporo 060, Japan.]

Swann, H., 1996: Investigation of different representations of rain in a 1-D evaporation model. Joint Centre for Mesoscale Meteorology Internal Rep. 59, 21 pp. [Available from Joint Centre for Mesoscale Meteorology, Harry Pitt Bldg., University of Reading, Whiteknights Rd., P.O. Box 240, Reading, Berkshire RG6 6FN, United Kingdom.]

Szoke, E. J., E. J. Zipser, and D. P. Jorgensen, 1986: A radar study of convective cells in mesoscale systems in GATE. Part I: Vertical profile statistics and comparisons with hurricanes. *J. Atmos. Sci.,* **43,** 182–197.

Takayabu, Y. N., 1994: Large-scale cloud disturbances associated with equatorial waves. Part II: Westward propagating inertio-gravity waves. *J. Meteor. Soc. Japan,* **72,** 451–465.

——, K.-M. Lau, and C.-H. Sui, 1996: Two-day variation in cloud–atmosphere coupled system observed in TOGA COARE IOP. *Mon. Wea. Rev.,* **124,** 1892–1913.

Taylor, R. C., 1973: An atlas of Pacific islands rainfall. Rep. HIG-73-9, 7 pp. [Available from Hawaii Institute of Geophysics, 2525 Correa Rd., Honolulu, HI 96822.]

TOGA COARE International Project Office, 1992: TOGA COARE operations plan. Working Version, University Corporation for Atmospheric Research, 500 pp. [Available from UCAR, P.O. Box 3000, Boulder, CO 80307-3000.]

TOGA COARE, 1993: TOGA COARE IOP operations summary. TOGA COARE International Project Office, 493 pp. [Available from the TOGA COARE International Project Office, UCAR, P.O. Box 3000, Boulder, CO 80307-3000.]

Tokay, A., and D. A. Short, 1996: Evidence from tropical raindrop spectra of the origin of rain from stratiform versus convective clouds. *J. Appl. Meteor.,* **35,** 355–371.

——, ——, and B. Fisher, 1995: Convective versus stratiform precipitation classification from surface measured drop size distributions at Darwin, Australia and Kapingamarangi Atoll. *Proc. 27th Conf. on Radar Meteorology,* Vail, CO, Amer. Meteor. Soc., 690–693.

Veldon, C. S., and J. A. Young, 1994: Satellite observations during TOGA COARE: Large-scale descriptive overview. *Mon. Wea. Rev.,* **122,** 2426–2441.

Webster, P. J., and R. Lukas, 1992: TOGA COARE: The Coupled Ocean–Atmosphere Response Experiment. *Bull. Amer. Meteor. Soc.,* **73,** 1377–1416.

——, C. A. Clayson, and J. A. Curry, 1996: Clouds, radiation, and the diurnal cycle of sea surface temperature in the western tropical Pacific. *J. Climate,* **9,** 1712–1730.

Weller, R. A., and S. P. Anderson, 1996: Surface meteorology and air–sea fluxes in the western equatorial Pacific warm pool during the TOGA Coupled Ocean–Atmosphere Response Experiment. *J. Climate,* **9,** 1959–1990.

Wilkerson, J., 1994: Rain gauge calibration and testing. *Optical Rain Gauge Performance, Second Workshop on Optical Rain Gauge Measurements,* D. A. Short, O. W. Thiele, and M. J. McPhaden, Eds., NASA Conference Publications, 53–61.

Williams, C. R., W. L. Ecklund, and K. S. Gage, 1995: An algorithm for classifying rain in the Tropics using a 915 MHz wind profiler. *J. Atmos. Oceanic Technol.,* **12,** 996–1012.

Willis, P. T., R. A. Block, and F. D. Marks Jr., 1995: Airborne raindrop size distributions in TOGA COARE. Preprints, *21st Conf. on Hurricanes,* Miami, FL, Amer. Meteor. Soc., 431–433.

World Climate Research Programme, 1990: Scientific Plan for the TOGA Coupled Ocean-Atmosphere Response Experiment. Publications Series No. 3, Addendum, 103 pp.

Yuter, S. E., and R. A. Houze Jr., 1997: Measurements of raindrop size distributions over the Pacific warm pool and implications for *Z–R* relations. *J. Appl. Meteor.,* **36,** 847–867.

——, ——, B. F. Smull, F. D. Marks Jr., J. R. Daugherty, and S. R. Brodzik, 1995: TOGA COARE aircraft mission summary images: An electronic atlas. *Bull. Amer. Meteor. Soc.,* **76,** 319–328.

Zawadski, I., 1975: On radar–raingage comparison. *J. Appl. Meteor.,* **14,** 1430–1436.

Zipser, E. J., 1969: The role of organized unsaturated convective downdrafts in the structure and rapid decay of an equatorial disturbance. *J. Appl. Meteor.,* **8,** 799–814.